Electronic Supplementary Material (ESI) for Materials Chemistry Frontiers.

Supporting Information

Porous RuO_2-Co_3O_4/C nanocubes as high-performance trifunctional electrocatalyst for zinc-air battery and overall water splitting

Jingyi Shi,[a]† Niannian Wang,[b]† Wenhao Du,[b] Yi Feng*[c] and Xin-Yao Yu*[ad]

[a]*Institutes of Physical Science and Information Technology, Institute of Energy, Hefei Comprehensive National Science Centre (Anhui Energy Laboratory), Anhui University, Hefei 230601, P. R. China. E-mail: yuxinyao@ahu.edu.cn*

[b]*Wendian College, Anhui University, Hefei 230601, P. R. China.*

[c]*Department of Polymer Materials and Engineering, Academy of Chemical Engineering, Hebei University of Technology, Tianjin 300130, P. R. China. Email: luckyii0512@hebut.edu.cn*

[d]*School of Materials Science and Engineering, Anhui University, Hefei 230601, P. R. China.*

†These two authors contribute equally to this work.

Experimental

Chemicals:

Cobalt(III) nitrate hexahydrate ($Co(NO_3)_2 \cdot 6H_2O$), 2-methylimidazole ($C_4H_6N_2$), hexadecyltrimethylammonium bromide (CTAB), Ruthenium(III) chloride hydrate (Cl_3H_2ORu, AR, 98%), hydrochloric acid (HCl, AR), and anhydrous ethanol (AR) were obtained from Shanghai Maclin. The water used was deionized water (DIW). All purchased chemicals were not further purified and all solvents were analytical grade.

Synthesis of ZIF-67 nanocubes:

The ZIF-67 nanocubes were synthesized at room temperature. In a typical synthesis, 116 mg of $Co(NO_3)_2 \cdot 6H_2O$ and 2 mg of CTAB were dissolved in 4 mL of DIW (solution A). Meanwhile, 1.816 g of 2-Methylimidazole was dissolved in 28 mL of DIW (solution B). Then, Solution A was added into solution B slowly. After stirring at room temperature for 25 min, the resulting solution was centrifuged and the collected products were washed with ethanol for six times and then dried at 60 ℃ overnight to obtain ZIF-67 powder.

Synthesis of Co/C and RuCo/C nanocubes:

An appropriate amount of ZIF-67 powders was calcined in N_2 atmosphere at a calcination temperature of 800 ^{o}C for 3 h and a heating rate of 5 ^{o}C min^{-1}. The Co/C nanocubes were then obtained. As control samples, the ZIF-67 powders were also carbonized at the temperature of 700 ^{o}C and 900 ℃ and the resultant products were named Co/C-700 and Co/C-900, respectively. Subsequently, 40 mg of Co/C were weighed and fully dispersed into 40 ml of DIW. After adding 16 mg of $RuCl_3 \cdot xH_2O$, the resulting solution was stirred at room temperature for 6 h. Finally, the products were washed with DIW for 3 times and dried to get RuCo/C. The products obtained by reacting RuCo/C-700 and RuCo/C-900 with 16 mg of $RuCl_3 \cdot xH_2O$ were denoted as RuCo/C-700 and RuCo/C-900. As control samples, 40 mg of Co/C were also reacted with 8 mg and 32 mg of $RuCl_3 \cdot xH_2O$ and the resultant products were denoted as RuCo/C-1 and RuCo/C-2, respectively.

Synthesis of RuCoO/C and Co_3O_4/C nanocubes:

The Co/C, RuCo/C, RuCo/C-700, RuCo/C-900, RuCo/C-1, and RuCo/C-2 nanocubes were calcined in air at 300 °C for 3 h to obtain Co_3O_4/C, RuCoO@C, RuCoO/C-700, RuCoO/C-900, RuCoO/C-1, and RuCoO/C-2 nanocubes, respectively. As control samples, the RuCo/C nanocubes were also calcined at 200 and 400 °C and the obtained products are named as RuCoO/C-200 and RuCoO/C-400, respectively.

Materials characterizations:

The morphology of the materials was characterized by scanning electron microscopy (SEM, Hitachi S-4800) and transmission electron microscope (TEM, JEOL Japan Electronics Co., Ltd JEM-2100F). The crystal structure of the materials was measured on X-ray diffraction instrument (XRD, BRUKER D2phaser). The surface elements and chemical valence states were characterized by X-ray photoelectron spectroscopy (XPS, Thermo Fisher Scientific ESCALAB250). The amount of hydrogen production was monitored by Gas chromatography (GC9790). The Raman spectra of materials were measured by Thermo Fisher Scientific DXR Smart Raman.

Electrochemical measurements:

All the electrochemical measurements were carried out by using CHI760E and Biologic multi-channel electrochemical workstations at room temperature. In the three-electrode test system, the Hg/HgO electrode and carbon rod electrode were utilized as reference and counter electrodes, respectively. The rotation ring disc electrode (RRDE) covered with catalyst (0.3 mg cm^{-2}) was used as working electrode for the ORR activity test. The rotation disc electrode (RDE) covered with catalysts (0.35 mg cm^{-2}) were used as working electrodes for the OER and HER activity tests. The catalyst ink was prepared by dispersing 5 mg of catalyst in the mixture of 270 μL of ethanol, 200 μL of deionized water, and 30 μL of Nafion solution (5 wt%) with sonication for 30 min. After that, a certain amount of uniformly dispersed catalyst ink was dropped onto the RDE or RRDE. Finally, the RDE/RRDE was dried at room temperature for further characterization. The RDE/RRDE was rotated at 1600 rpm during electrocatalytic tests. All potentials were given with respect to the reversible hydrogen electrode (RHE):

E (*vs*. RHE) = E (*vs*. Hg/HgO) + 0.098 V + 0.0592 × pH.

The ORR performance was evaluated in 0.1 M KOH. During ORR activity test, the scan rates of CV curves and LSV curves were 50 and 5 mV s^{-1}, respectively. In the ORR stability test, the catalysts supported on RRDE was used as the working electrode and the applied voltage was fixed at 0.6 V. The transferred electron numbers of ORR is calculated by the *K-L* equation provided as follows:

$1/J = 1/J_K + 1/(B\omega^{1/2})$

Where J is the measured current density, J_K is the kinetic limiting current density, and ω is the rotating rate. B can be calculated from the Levich slope below:

$B = 0.2nFC_0D_0^{2/3}\, v^{-1/6}$

In this equation, n is the transferred electron numbers, F is Faraday constant (F = 96485 C mol^{-1}), and C_0 is the concentration of O_2 in the solution ($C_0 = 1.2 \times 10^{-6}$ mol cm^{-3}). D_0 is the diffusion coefficient of O_2 in 0.1 M KOH ($D_0 = 1.9 \times 10^{-5}$ cm^2 s^{-1}) and v is the kinematics viscosity of the electrolyte ($v = 0.01$ cm^2 s^{-1}).

In addition, the RRDE was also used to evaluate the electron tarnsfer number (n) which could be calculated by the following Equation: $n = 4|I_d|\ (|I_d|+I_r/N_c)^{-1}$

Where the I_d, I_r, and N_c (0.38) is the current of the disk, the current of ring, and the collection efficiency of the Pt ring, respectively.

The OER performance was evaluated in both 0.1 M and 1 M KOH. The HER performance was evaluated in 1 M KOH. The scan rate of LSV curves during OER and HER test was 5 mV s^{-1}. The alkaline seawater was prepared by mixing the KOH solution with the natural seawater (Qingdao, China) and adjusting the pH of the mixed electrolyte to 14. It is mainly composed of NaCl, $MgCl_2$, $MgSO_4$, and K_2SO_4. No other pretreatment was performed after natural seawater filtration. In the OER and HER stability test, the catalysts were dropped onto Ni foam with a loading of 5 mg cm^{-2}. In the overall water splitting test, the catalysts were loaded on Ni foam. And the catalysts loading for the OER and HER sides were 2 and 0.5 mg cm^{-2}, respectively. The scan rate of LSV curves for the overall water splitting test was 5 mV s^{-1}.

The FE for OER was determined by RRDE. The generated O_2 molecules were detected by oxygen reduction reaction when the ring potential was 0.53 V. The FE value of O_2 was calculated using the following formula:

$$FE = \frac{I_{ring}}{I_{disk} \cdot N_c}$$

Where I_{ring} means the ring current, I_{disk} refers to the disk current, and N_c represents the collection efficiency (here is 0.38).

The actual amount of H_2 generated on the working electrode is directly obtained by gas chromatography: $n(H_2)_{exp} = x_o \times n$, where x_o represents the amount of hydrogen generated (mol ppm^{-1}) and n refers to the amount of hydrogen produced in 1 cm^3. The amount of H_2 produced theoretically during the HER process is obtained by the following formula: $n(H_2)_{tho} = It/2F$. The calculation equation for Faraday efficiency is as follows: FE = $n(H_2)_{exp} / n(H_2)_{tho} \times 100\%$.

The C_{dl} method was used to estimate the ECSA. As for C_{dl}, it was acquired by cyclic voltammetry method at different scanning rates between 1.2 and 1.3 V *vs.* RHE (4-20 mV s^{-1}). The differences of current densities at 1.25 V vs. RHE were plotted as a function of scan rates. The slope of the fitted line was equal to half of the C_{dl}. The EIS tests were collected at an amplitude of 5 mV as well as frequency range of 10^5~0.1 Hz.

Aqueous Zn-air batteries and flexible Zn-Air batteries assembly and measurements: In liquid ZABs, carbon cloth supported with catalyst was taken as the negative electrode, zinc foil as the positive electrode, and the mixed solution containing 6.0 M KOH and 0.2 M $Zn(CH_3COO)_2$ as the electrolyte. The working electrode was prepared by evenly dispersing 20 mg of the catalyst (20 mg for RuCoO/C; 10 mg + 10 mg for Pt/C and RuO_2) into a mixture containing 652 μL of isopropyl alcohol, 261 μL of deionized water, and 87 μL of Nafion solution, then removing 50 μL of the catalyst and coating it evenly on a carbon cloth. The electrolyte for solid ZABs was prepared as follows: 1 g of polyvinyl alcohol was first dissolved in 10 mL of deionized water and heated at 90 ^{o}C for 1 h. Then, 1 mL of 18 M KOH + 0.2 M $Zn(CH_3COO)_2$ solution was added and continued to heating for 1 h. Finally, the above solution was freeze-dried for 2 h and then returned to room temperature. ZABs performance tests were performed on CHI760E and Biologic multi-channel electrochemical workstations.

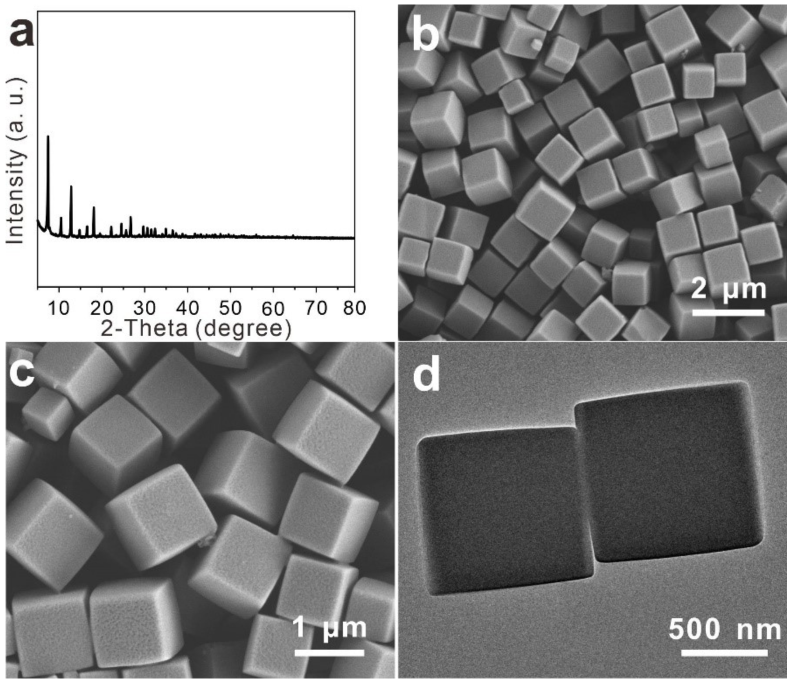

Fig. S1. (a) XRD pattern, (b,c) SEM images, and (d) TEM image of ZIF-67.

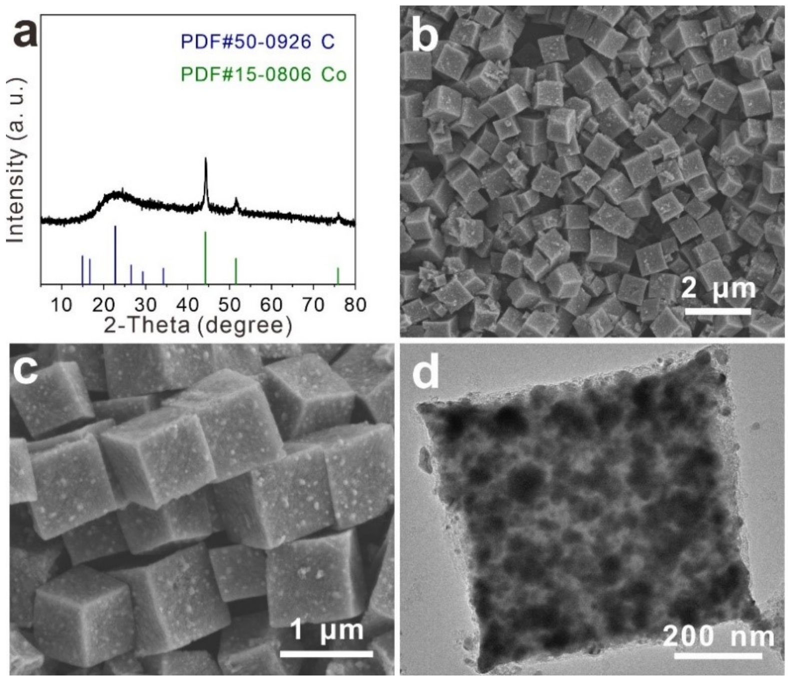

Fig. S2. (a) XRD pattern, (b,c) SEM images, and (d) TEM image of Co/C .

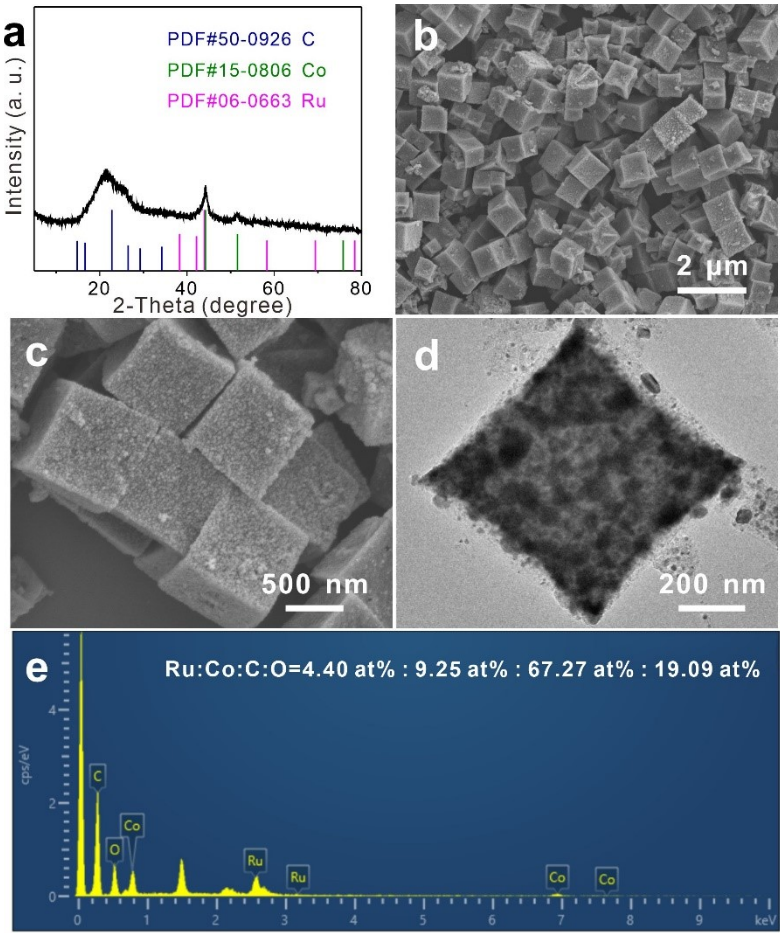

Fig. S3. (a) XRD pattern, (b,c) SEM images, (d) TEM image, and (e) EDS spectrum of RuCo/C.

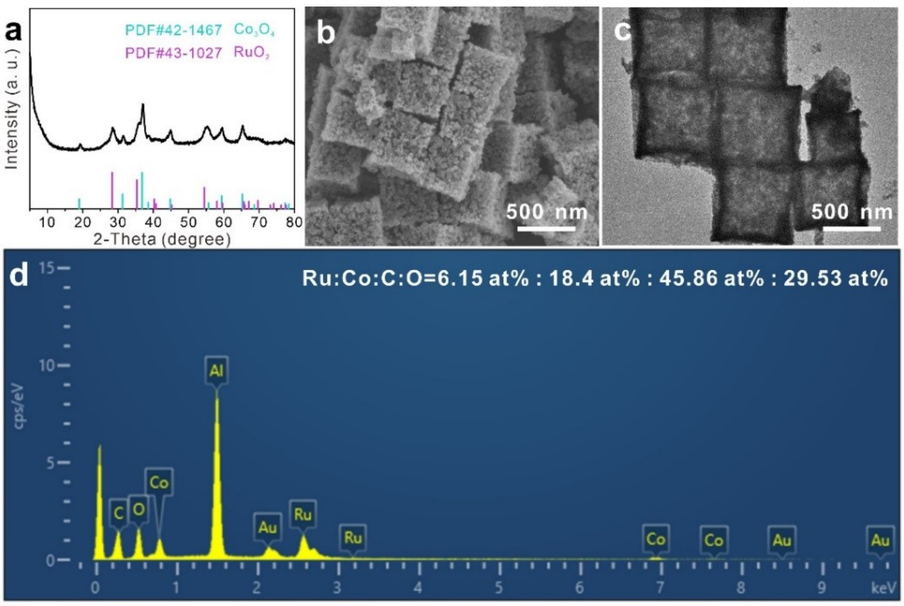

Fig. S4. (a) XRD pattern, (b) SEM image, and (d) EDS spectrum of RuCoO/C. The Al signal comes from the substrate used for EDS test.

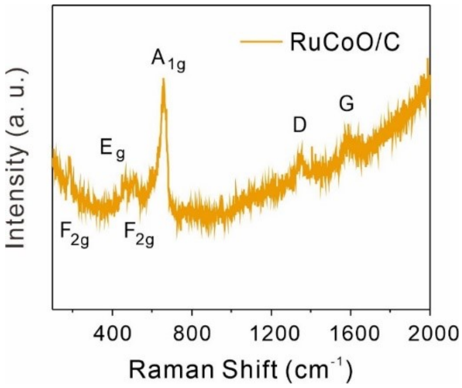

Fig. S5. Raman spectra of RuCoO/C.

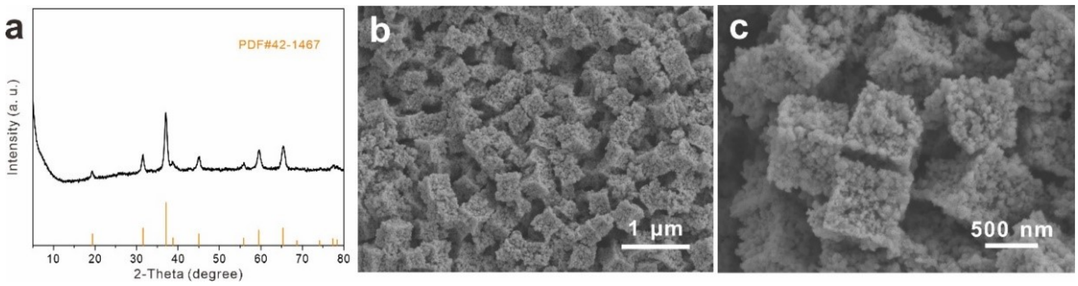

Fig. S6. (a) XRD pattern and (b,c) SEM images of Co_3O_4/C.

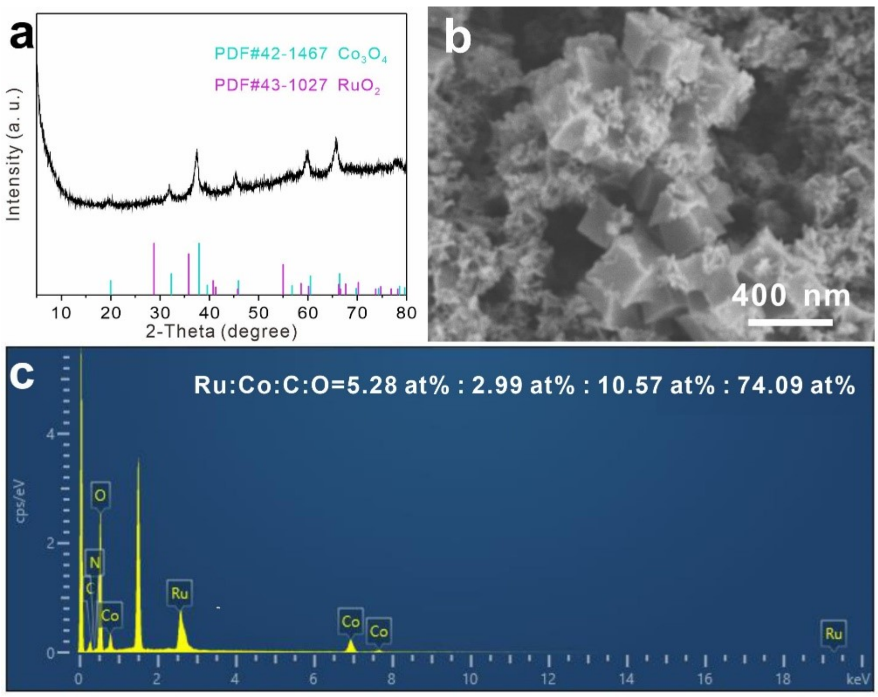

Fig. S7. (a) XRD pattern, (b) SEM image, and (c) EDS spectrum of RuCoO.

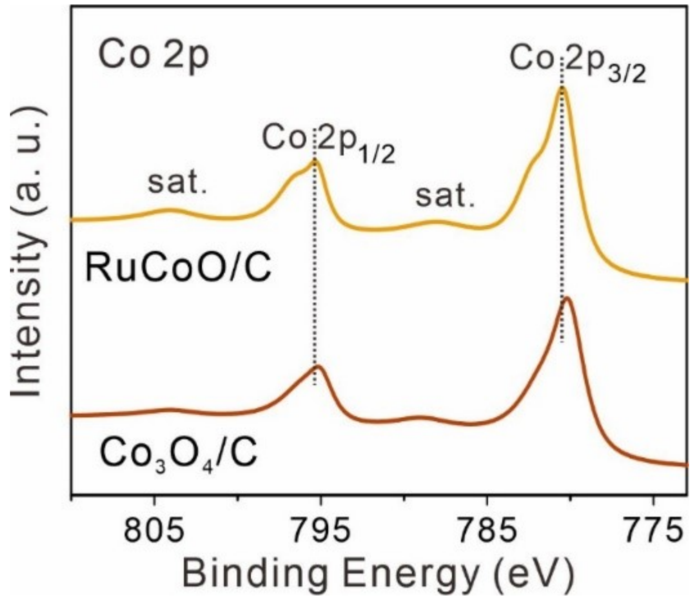

Fig. S8. High-resolution Co 2p XPS spectra of RuCoO/C and Co_3O_4/C.

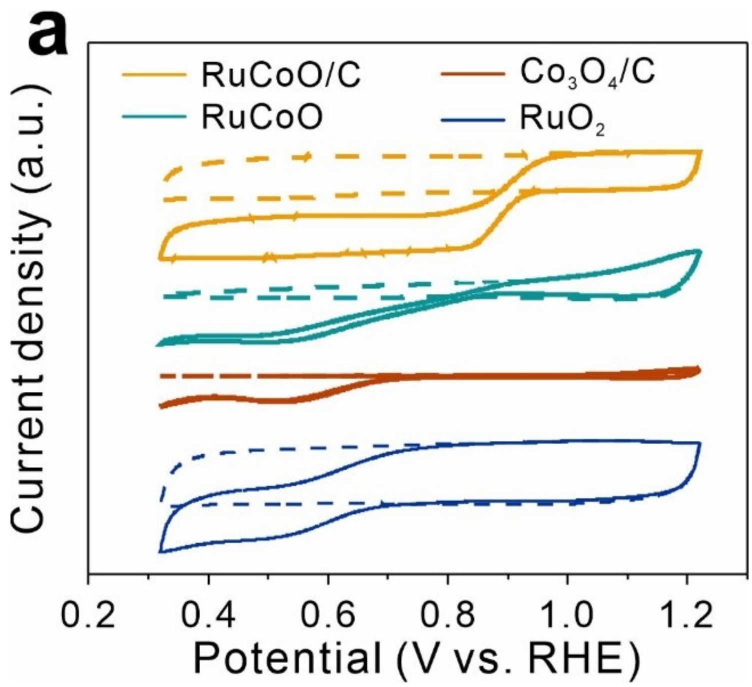

Fig. S9. CV curves of RuCoO/C, Co_3O_4/C, RuCoO, and RuO_2 tested in N_2-saturated (dash line) and O_2-saturated (solid line) 0.1 M KOH electrolyte.

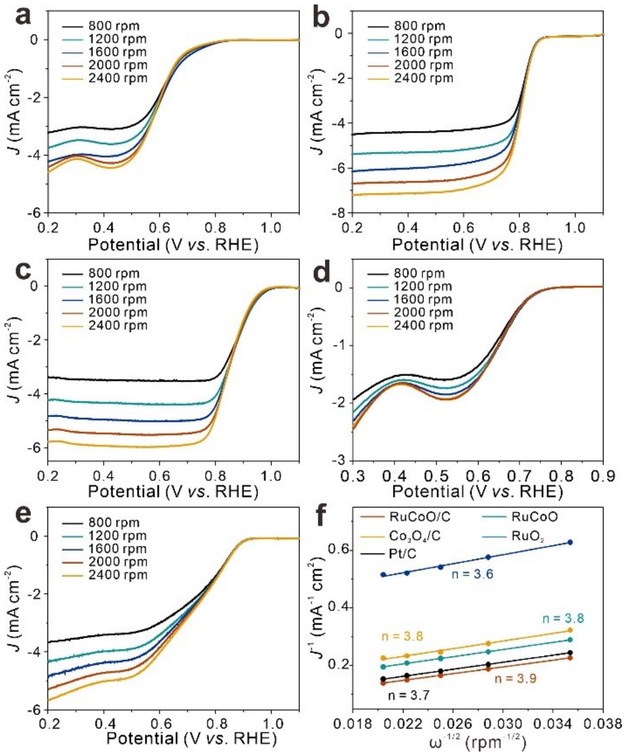

Fig. S10. LSV curves at different rotation rates from 800 to 2400 rpm in ORR region of (a) Co_3O_4/C, (b) RuCoO/C, (c) Pt/C, (d) RuO_2, and (e) RuCoO. (f) *K-L* plots of Co_3O_4/C, RuCoO/C, Pt/C, RuO_2, and RuCoO.

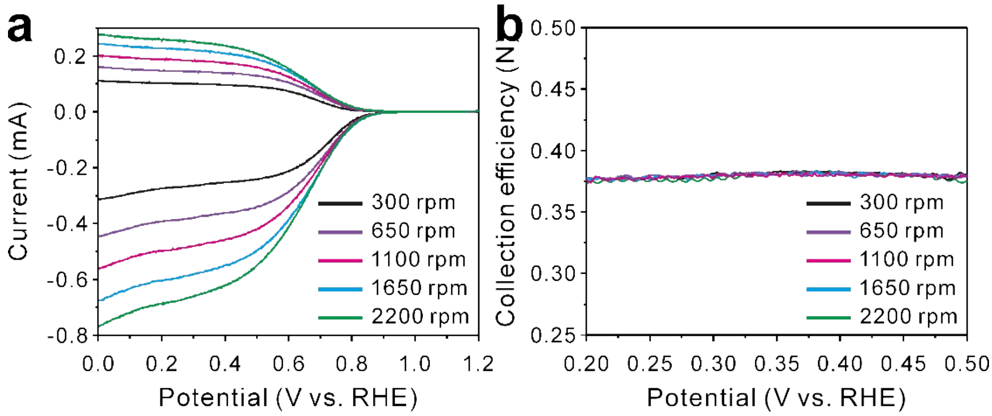

Fig. S11. (a) Linear sweep voltammetry curves recorded on a bare glassy carbon rotation disk electrode with a Pt ring in the electrolyte containing 0.05 M Na_2SO_4 and 4 mM $K_3Fe(CN)_6$ at 300, 650, 1100, 1650, and 2200 rpm. (b) The experimental determined collection efficiency (N_c) via dividing the ring current by the disk ring in (a).

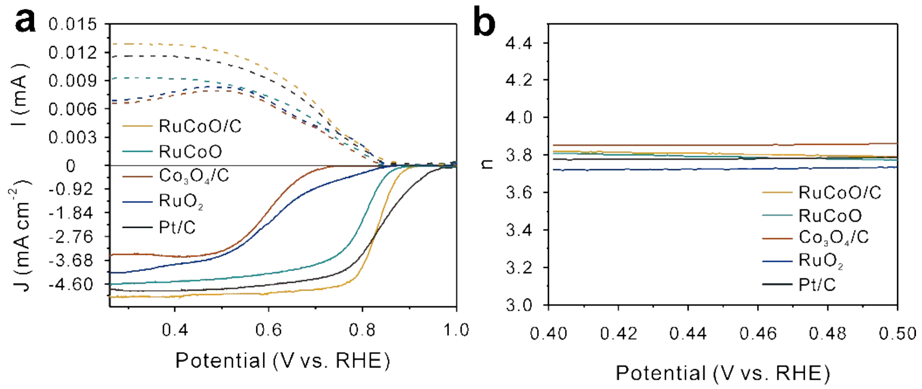

Fig. S12. (a) LSV curves of disk (solid line) and ring (dash line) and (b) electron transfer number (n) of RuCoO/C, RuCoO, Co_3O_4, RuO_2, and Pt/C.

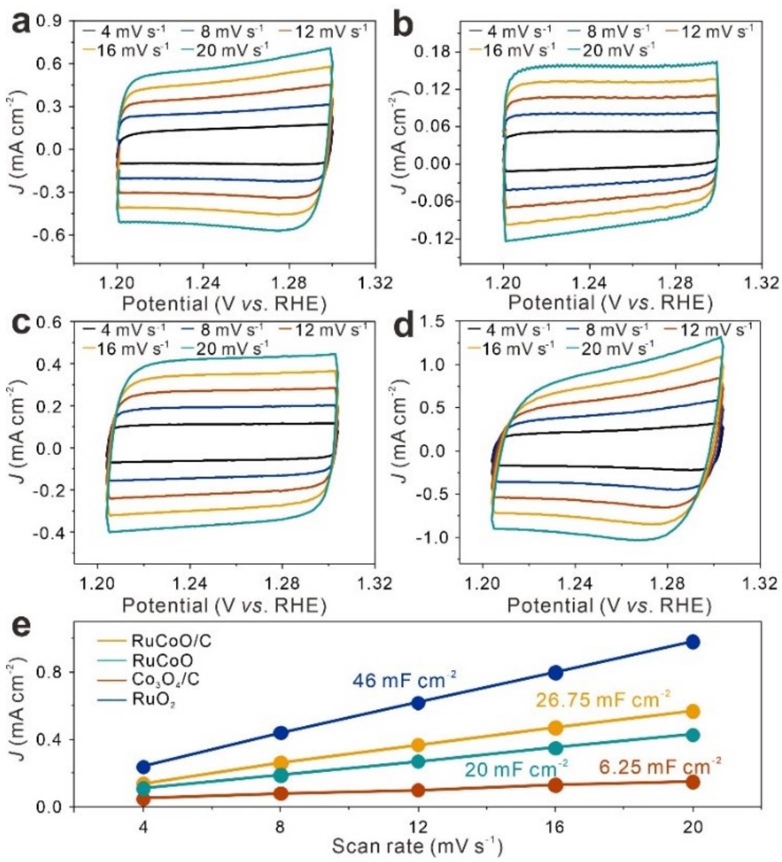

Fig. S13. CV curves at different scan rates from 4 to 20 mV s^{-1} of (a) RuCoO/C, (b) Co_3O_4/C, (c) RuCoO, and (d) RuO_2, (e) C_{dl} of RuCoO/C, Co_3O_4/C, RuCoO, and RuO_2.

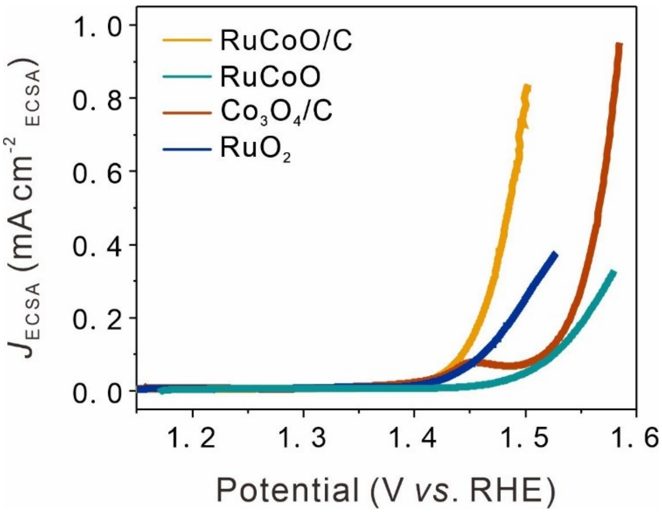

Fig. S14. ECSA-normalized LSV curves of RuCoO/C, RuCoO, Co_3O_4/C, and RuO_2.

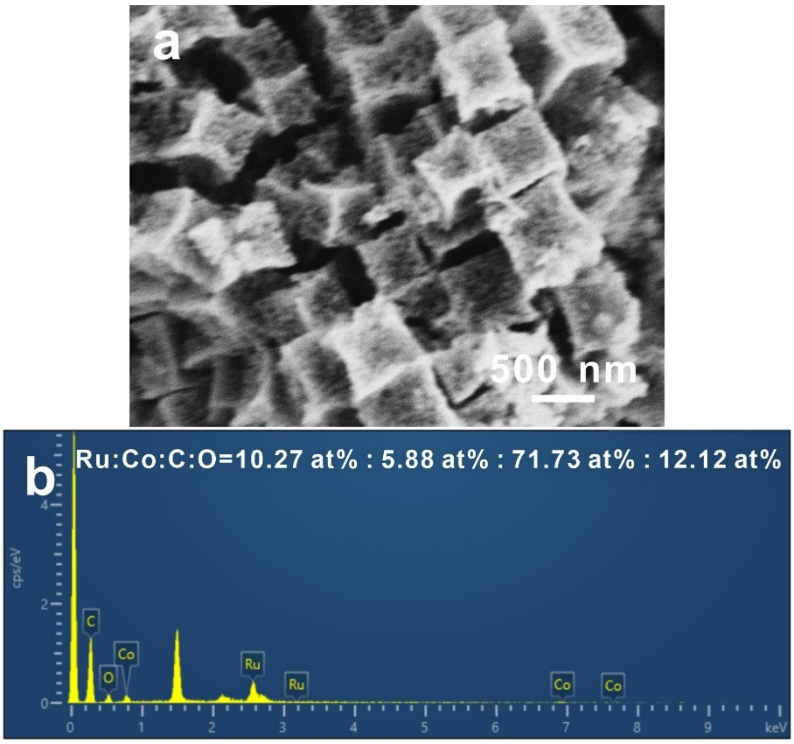

Fig. S15. (a) SEM image and (b) EDS spectrum of RuCoO/C after ORR stability test in 0.1 M KOH.

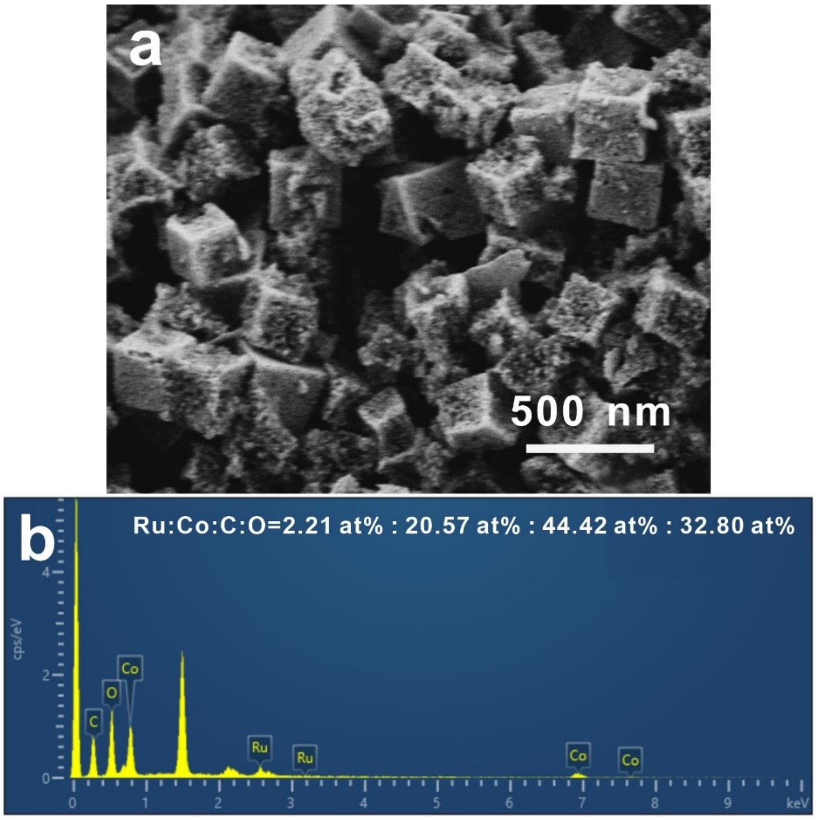

Fig. S16. (a) SEM image and (b) EDS spectrum of RuCoO/C after OER stability test in 0.1 M KOH.

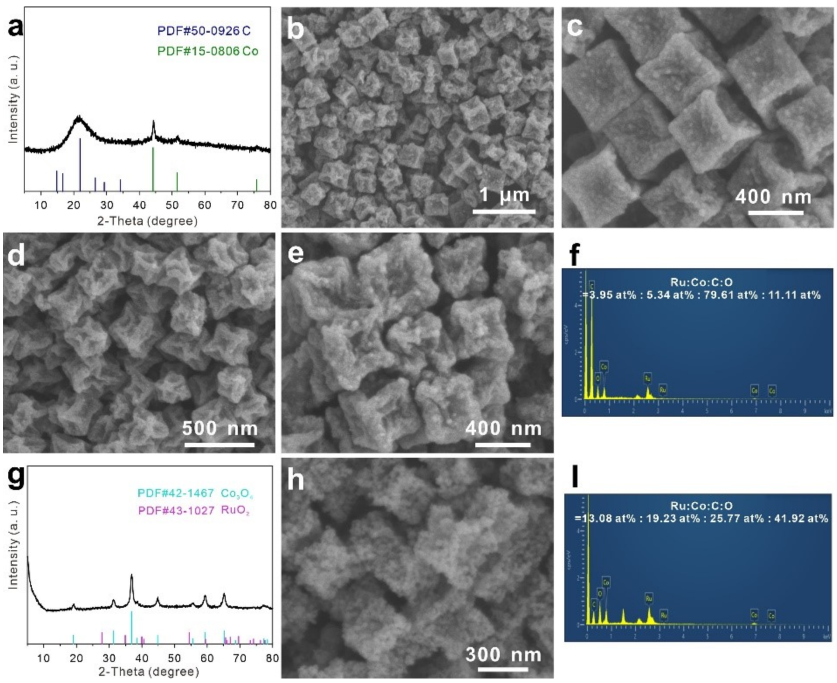

Fig. S17. (a) XRD pattern and (b,c) SEM images of Co/C-700. (d,e) SEM images and (f) EDS spectrum of RuCo/C-700. (g) XRD pattern, (h) SEM image, and (i) EDS spectrum of RuCoO/C-700.

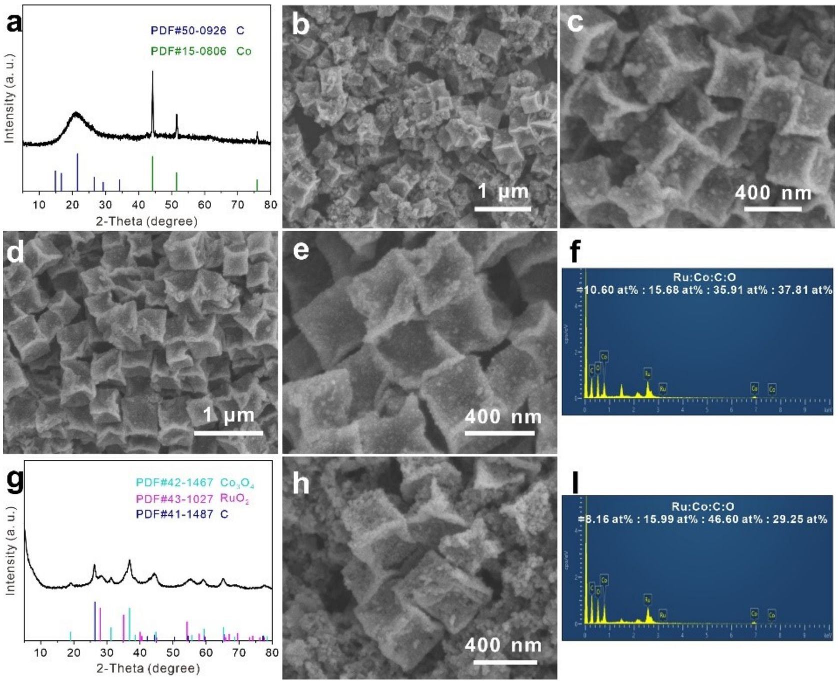

Fig. S18. (a) XRD pattern and (b,c) SEM images of Co/C-900. (d,e) SEM images and (f) EDS spectrum of RuCo/C-900. (g) XRD pattern, (h) SEM image, and (i) EDS spectrum of RuCoO/C-900.

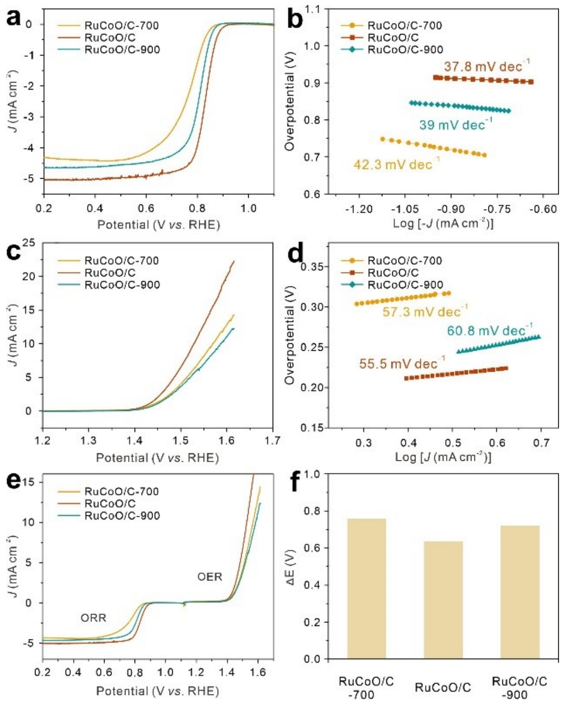

Fig. S19. Bifunctional activity of RuO_2-Co_3O_4/C synthesized at different carbonization temperatures: (a,c) LSV curves and (b,d) Tafel plots of ORR (a,b) and OER (c,d); (e) Overall LSV curves and (f) values of potential gap. RuCoO/C is the synthesized at the carbonization of 800 ^oC.

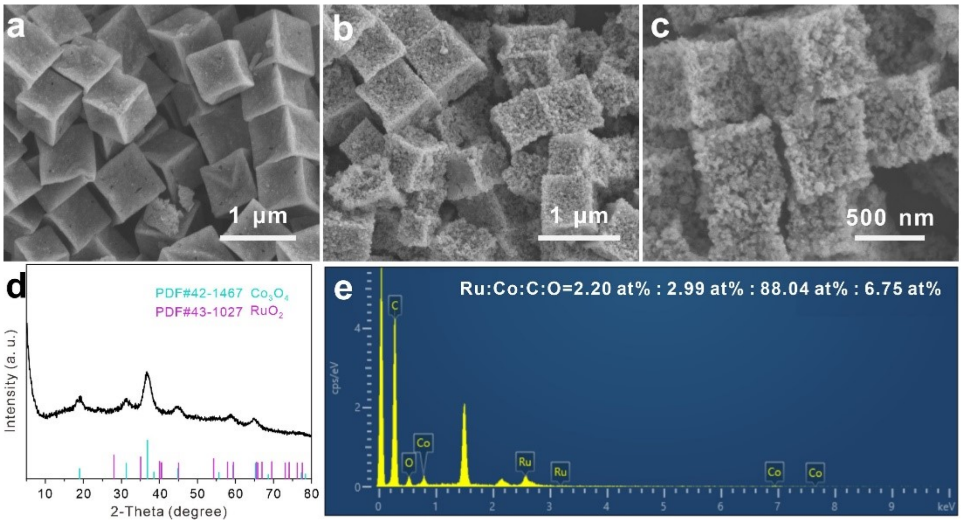

Fig. S20. (a) SEM image of RuCo/C-1. (b,c) SEM images, (d) XRD pattern, and (e) EDS spectrum of RuCoO/C-1.

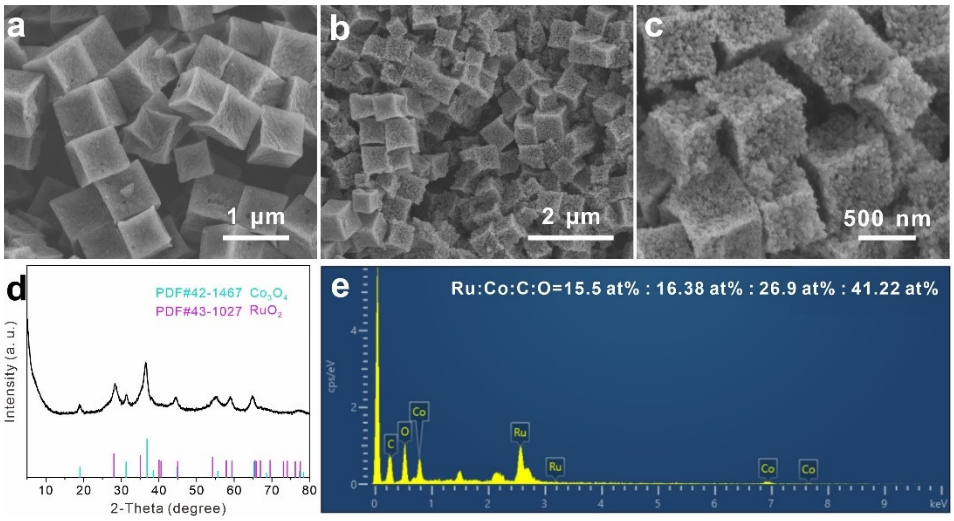

Fig. S21. (a) SEM image of RuCo/C-2. (b,c) SEM images, (d) XRD pattern, and (e) EDS spectrum of RuCoO/C-2.

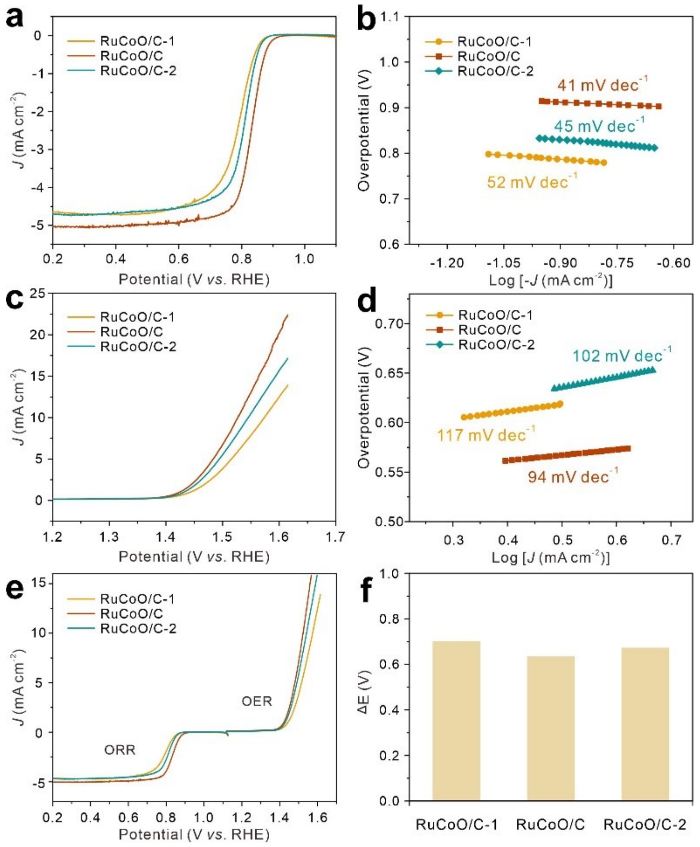

Fig. S22. Bifunctional activity of RuO_2-Co_3O_4/C with different Ru loading: (a,c) LSV curves and (b,d) Tafel plots of ORR (a,b) and OER (c,d); (e) Overall LSV curves and (f) values of potential gap.

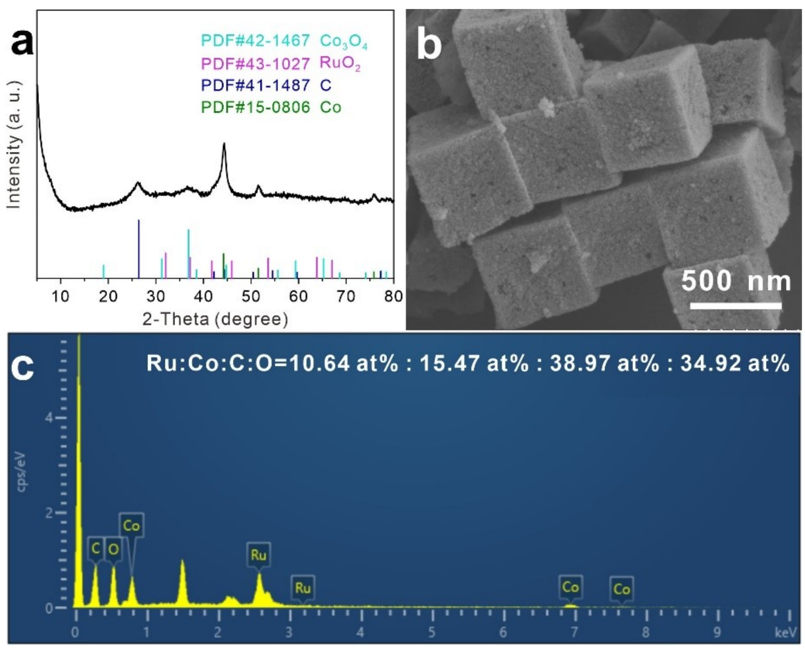

Fig. S23. (a) XRD pattern, (b) SEM image, and (c) EDS spectrum of RuCoO/C-200.

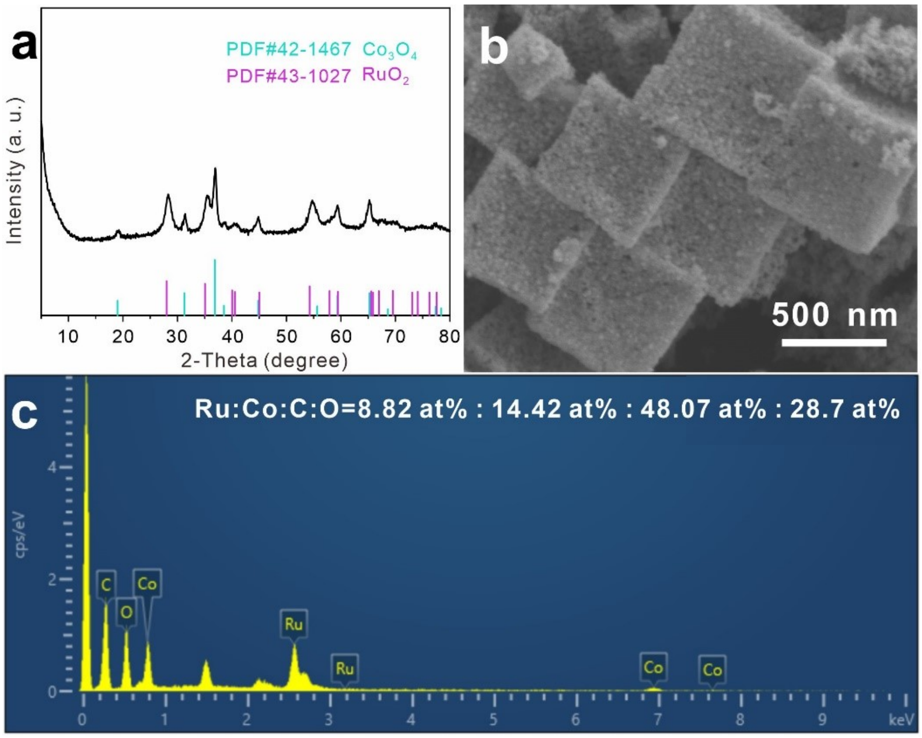

Fig. S24. (a) XRD pattern, (b) SEM image, and (c) EDS spectra of RuCoO/C-400.

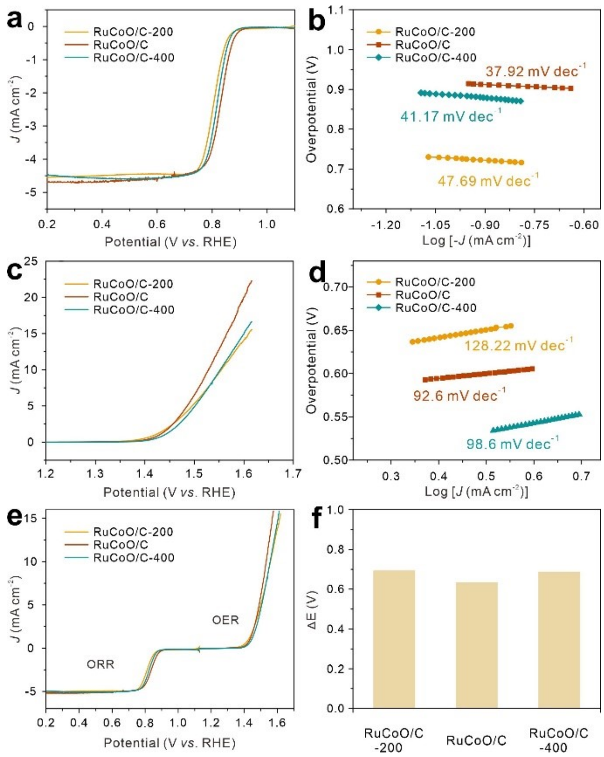

Fig. S25. Bifunctional activity of RuO_2-Co_3O_4/C obtained at different oxidation temperature: (a,c) LSV curves and (b,d) Tafel plots of ORR (a,b) and OER (c,d); (e) Overall LSV curves and (f) values of potential gap.

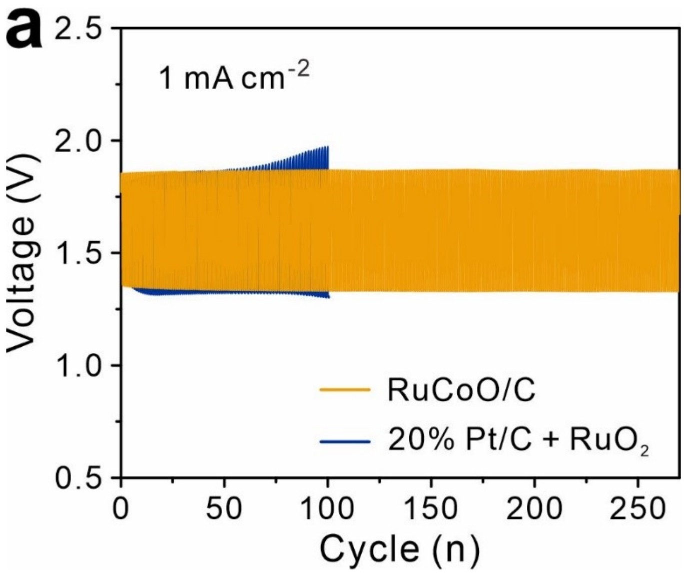

Fig. S26. Galvanostatic charge/discharge curves of aqueous ZABs at 1 mA cm^{-2}.

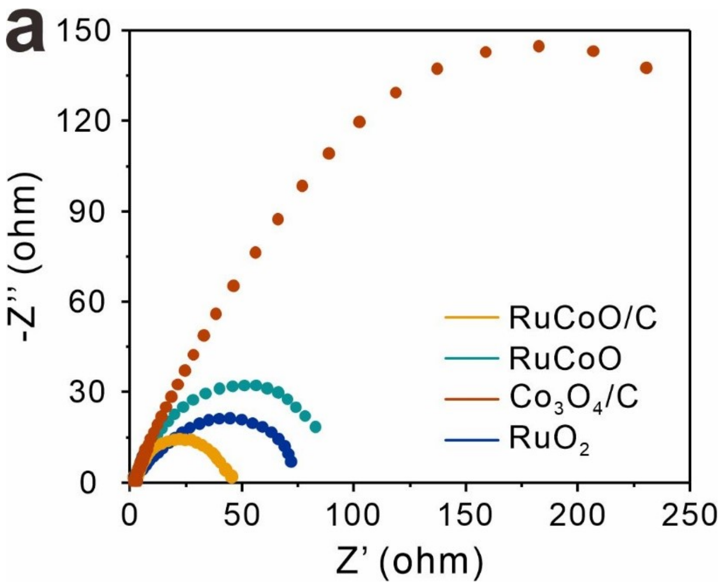

Fig. S27. Nyquist plots of RuCoO/C, RuCoO, Co_3O_4/C, and RuO_2 in 1 M KOH at the overpotential of 287 mV.

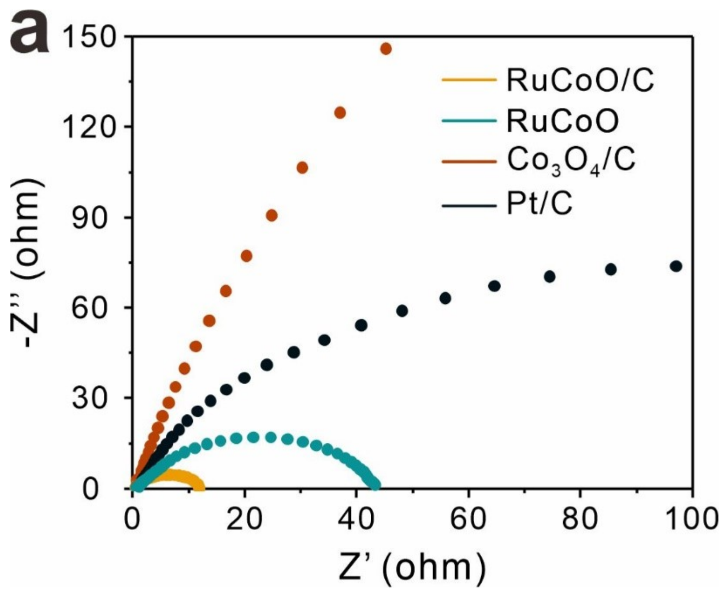

Fig. S28. Nyquist plots of RuCoO/C, RuCoO, Co_3O_4/C, and Pt/C in 1 M KOH at the overpotential of -50 mV.

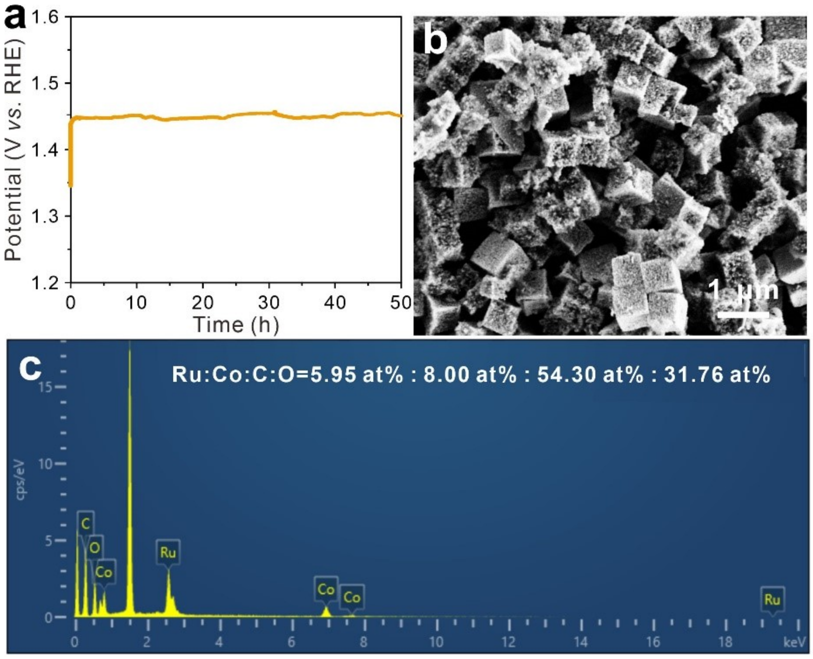

Fig. S29. (a) Chronopotentiometry response at 10 mA cm^{-2} for OER; (b) SEM image, (c) EDS spectrum of RuCoO/C after OER stability test in 1 M KOH.

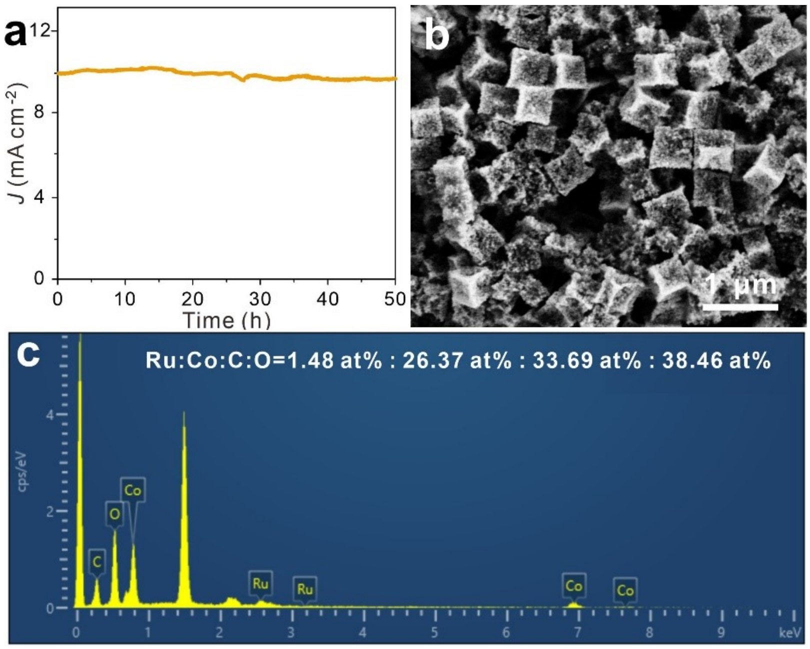

Fig. S30. (a) Chronoamperometric response at the overpotential of 10 mA cm^{-2} for HER; (b) SEM image, (c) EDS spectrum of RuCoO/C after HER stability test in 1 M KOH.

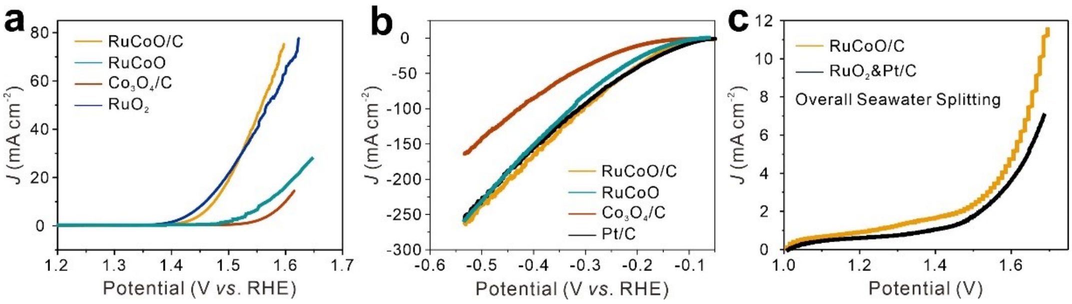

Fig. S31. OER and HER performance of RuCoO/C in 1 M KOH + Seawater. LSV curves of (a) OER and (b) HER. (c) The overall water splitting performance of RuCoO/C 1 M KOH + Seawater.

Table S1. Comparison for ORR/OER/HER of RuCoO/C with other reported catalysts.

The catalyst	ORR (V) Half wave potential	OER (mV) at 10 mA cm^{-2}	HER (mV) at 10 mA cm^{-2}	Ref.
RuCoO/C	**0.83@0.1 M KOH**	**223@1 M KOH**	**49@1 M KOH**	**This work**
ZnCo–PVP-900	0.84@0.1 M KOH	350@1 M KOH	150@1 M KOH	[1]
CoFeNi-342	0.86@0.1 M KOH	430@1 M KOH	547@1 M KOH	[2]
$CoO_x/CoN_y@CN_{z,700}$	0.82@1 M KOH	280@1 M KOH	261.4@1 M KOH	[3]
Co_9S_8-MoS_2/N-CNAs@CNFs	0.82@0.1 M KOH	340@1 M KOH	163@1 M KOH	[4]
Cu-14-Co_3Se_4/GC	0.89@0.1 M KOH	280@1 M KOH	166@1 M KOH	[5]

References:

[1] Chen Deng, Kuang-Hsu Wu, Jason Scott, Shenmin Zhu, Xianfeng Zheng, Rose Amal and Da-Wei Wang. Spherical Murray-Type Assembly of Co–N–C Nanoparticles as a High-Performance Trifunctional Electrocatalyst. *ACS Applied Materials & Interfaces*, 2019, **11**, 9925-9933.

[2] Chao Han, Weijie Li, Wenxian Li, Limei Yang and Zhenguo Huang. CoFeNi based trifunctional electrocatalysts featuring in-situ formed heterostructure. *Inorganic Chemistry Communications*, 2023, **142**, 1387-7003.

[3] Jiameng Liu, Changbao Wang, Hongming Sun, Heng Wang, Feilong Rong, Linghao He, Yafei Lou, Shuai Zhang, Zhihong Zhang and Miao Du. CoO_x/CoN_y nanoparticles encapsulated carbon-nitride nanosheets as an efficiently trifunctional electrocatalyst for overall water splitting and Zn-air battery. *Applied Catalysis B: Environmental*, 2020, **279**, 119407.

[4] Wenming Zhang, Xinyan Zhao, Youwei Zhao, Jiaqing Zhang, Xiaoting Li, Lide Fang and Ling Li. Mo-Doped Zn, Co Zeolitic Imidazolate Framework-Derived Co_9S_8 Quantum Dots and MoS_2 Embedded in Three-Dimensional Nitrogen-Doped Carbon Nanoflake Arrays as an Efficient Trifunctional Electrocatalysts for the Oxygen Reduction Reaction. *ACS Applied Materials & Interfaces*, 2020, **12**, 10280–10290.

[5] Jiale Dai, Dengke Zhao, Wenming Sun, Xiaojing Zhu, Li-Jun Ma, Zexing Wu, Chenghao Yang, Zhiming Cui, Ligui Li and Shaowei Chen. Cu(II) Ions Induced Structural Transformation of Cobalt Selenides for Remarkable Enhancement in Oxygen/Hydrogen Electrocatalysis. *ACS Catalysis*, 2019, **9**, 10761–10772.